

Cosmic X-ray surveys of Active Galactic Nuclei: the synergy between X-ray and infrared observations

D. M. Alexander^{1,*}

¹ Centre for Extragalactic Astronomy, Department of Physics, Durham University, South Road, Durham, DH1 3LE, UK

Received DD MMM 2016, accepted DD MMM 2016

Published online later

Key words Editorial notes – instruction for authors

We briefly review the synergy between X-ray and infrared observations for Active Galactic Nuclei (AGNs) detected in cosmic X-ray surveys, primarily with *XMM-Newton*, *Chandra*, and *NuSTAR*. We focus on two complementary aspects of this X-ray–infrared synergy (1) the identification of the most heavily obscured AGNs and (2) the connection between star formation and AGN activity. We also briefly discuss future prospects for X-ray–infrared studies over the next decade.

© 2006 WILEY-VCH Verlag GmbH & Co. KGaA, Weinheim

1 Introduction

There is great synergy between X-ray and thermal infrared observations for the study of Active Galactic Nuclei (AGNs) and their connection to star formation (SF).¹

X-ray observations provide, arguably, the most efficient method currently available for reliably identifying AGNs. This is due to a combination of (1) the penetrating nature of X-rays, which allow even obscured AGNs to be directly identified at X-ray energies and (2) the low dilution from the host galaxy (i.e., X-ray emission associated to stellar processes) at X-ray energies. X-ray surveys of AGNs therefore provide one of the most complete and reliable approaches to construct a cosmic census of AGN activity (see Brandt & Alexander 2015 for a recent review). However, the most heavily obscured AGNs will be weak or undetected in X-rays, making their X-ray identification challenging or impossible. Furthermore, since the X-ray emission from the host galaxy is weak, X-ray surveys are not an effective method for providing a cosmic census of SF. Fortunately, these shortcomings can be mostly alleviated from a combination of thermal infrared and X-ray observations.

The thermal infrared waveband provides an effective method to study AGNs and their connection with SF (e.g., Alexander & Hickox 2012; Lutz 2014). The dust in the obscuring medium, which makes the heavily obscured AGNs weak or invisible at X-ray energies, will be heated by the AGN and emitted thermally at infrared wavelengths. Heavily obscured AGNs can therefore, in principle, be identified at infrared wavelengths. However, since a significant fraction of SF is also emitted at infrared wavelengths, due to the majority of stars forming in dusty molecular clouds (see Kennicutt & Evans 2012 for a review), the identification

of AGNs in the infrared waveband is often not a straightforward exercise. Fortunately, the AGN and SF components can often be distinguished in the infrared waveband since the AGN component has a “hotter” infrared energy distribution (SED; i.e., the AGN component is bright at mid-infrared wavelengths of $\approx 3\text{--}30\ \mu\text{m}$) and produces a harder ionisation radiation field than the SF component (e.g., Donley et al. 2012; Mateos et al. 2012; Stern et al. 2012; Assef et al. 2013). Therefore, several methods allow the infrared emission from the AGN component to be reliably measured even in the presence of SF at infrared wavelengths: (1) the decomposition of the SED into the AGN and SF components by fitting AGN and SF galaxy templates to the infrared emission, (2) high-spatial resolution infrared emission to isolate the AGN component at the centre of the galaxy from the SF emission (currently only possible for nearby AGNs), and (3) the detection of AGN and SF spectral “signatures” (i.e., emission lines and solid-state features) using infrared spectroscopy. Once the contribution from the AGN can be constrained at infrared wavelengths, the thermal infrared is arguably the most effective waveband for constructing the cosmic census of SF (e.g., Lutz 2014; Madau & Dickinson 2014).

The combination of X-ray and thermal infrared observations therefore provides the opportunity for a more complete understanding and cosmic census of AGN activity and the exploration and measurement of the connection between AGN activity and SF. In this short paper we briefly review recent results on the X-ray–infrared properties of AGNs and the identification of heavily obscured AGNs (see §2) and the connection between AGN activity and SF (see §3). We focus on results that use the most sensitive X-ray (*XMM-Newton* and *Chandra* at $< 10\ \text{keV}$ and *NuSTAR* at $> 10\ \text{keV}$; e.g., Jansen et al. 2001; Weisskopf et al. 2002; Harrison et al. 2013) and infrared (*Herschel*; ALMA; ground-based mid-infrared observatories: e.g., Pilbratt et al. 2010) observa-

* Corresponding author: e-mail: d.m.alexander@durham.ac.uk

¹ In this paper the thermal infrared waveband is defined as $3\text{--}1000\ \mu\text{m}$.

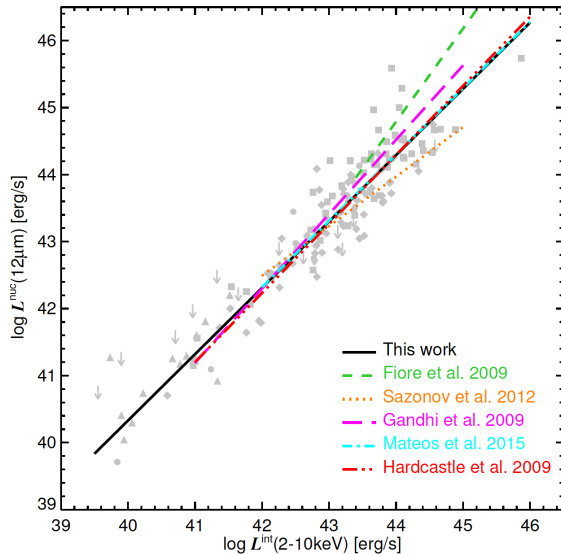


Fig. 1 Observed mid-infrared luminosity versus rest-frame 2–10 keV luminosity, demonstrating the intrinsic mid-infrared–X-ray relationship for nearby AGNs. The 2–10 keV luminosity has been corrected for the presence of absorption through detailed X-ray spectral modelling of the X-ray data and the mid-infrared observations are from high-spatial resolution 12 μm imaging at the location of the AGN. The black line shows the best-fitting relationship from Asmus et al. (2015) and the other lines show the best-fitting relationships from previous work (Fiore et al. 2009; Gandhi et al. 2009; Hardcastle et al. 2009; Sazonov et al. 2012; Mateos et al. 2015). Taken from Asmus et al. (2015).

tions available. In §4 we briefly review future prospects over the next decade.

2 X-ray and infrared synergy: AGN properties and the identification of heavily obscured AGNs

The combination of X-ray and thermal infrared observations provide insight on the properties of the AGN, in addition to allowing for a more complete census of AGNs over that obtained from just one of these wavebands. The X-ray emission is predominantly produced in the “corona” and is thought to be due to inverse Compton scattering of the primarily AGN accretion disc emission (which is produced mostly at ultra-violet–optical wavelengths) by electrons above the accretion disc (see Done 2010 for a review). By comparison, the infrared emission is predominantly due to heated dust grains in the obscuring structure (commonly referred to as the “torus” to indicate that it is geometrically thick) and is essentially the cooler outer regions of the accretion disc, where dust and molecules can form (see Elitzur & Shlosman 2006 for a review). Significant infrared emission is also produced in the narrow-line region of some AGNs, perpendicular to the accretion disc (e.g., Tristram

et al. 2014; López-Gonzaga et al. 2016). Given the different locations and sizes of the X-ray corona and infrared “torus”, the study of the X-ray and infrared emission from AGNs gives insight on the relative geometry of the corona–torus system (e.g., the covering factor of the obscuring “torus”).

In Fig. 1 we show the relationship between the observed 12 μm luminosity and the intrinsic (i.e., corrected for the presence of absorption) 2–10 keV luminosity for nearby AGNs. This plot is taken from Asmus et al. (2015), although the basic results are consistent with previous works but with significantly improved source statistics. The tightness of the infrared–X-ray luminosity relationship indicates that the corona–torus geometry is broadly constant and provides insight on the physical structure of the AGN. A corollary of this result is that the infrared emission from the AGN can be used to predict the intrinsic X-ray emission even when the AGN is so heavily obscured that it is weak or undetected at X-ray energies.² Consequently, the combination of X-ray and infrared observations can be used to identify the most heavily obscured AGNs known, including AGNs that are obscured by Compton-thick levels of absorption (i.e., when the absorbing column density is the inverse of the Thomson scattering cross section: $N_{\text{H}} > 1/\sigma_{\text{T}} > 1.5 \times 10^{24} \text{ cm}^{-2}$).

Many studies have combined infrared and X-ray observations of AGNs to identify the presence of Compton-thick absorbing column densities (e.g., Alexander et al. 2008; Bauer et al. 2010; Georgantopoulos et al. 2013). An example study is given in Fig. 2, which shows X-ray luminosity versus rest-frame 6 μm luminosity for a variety of AGNs studied from a combination of *XMM-Newton*, *Chandra*, and *NuSTAR* observations. In the left-hand plot the X-ray luminosity is at rest-frame 2–10 keV from *XMM-Newton* or *Chandra* while in the right-hand plot the X-ray luminosity is at rest-frame 10–40 keV from *NuSTAR*. The two main results from these plots are (1) there is a population of AGNs that are X-ray weak given their mid-infrared luminosity and (2) the X-ray “weakness” of these AGNs is less pronounced at 10–40 keV than at 2–10 keV. This X-ray weakness is likely to be due to extreme levels of absorption, which will effect the 2–10 keV emission more significantly than the 10–40 keV emission (e.g., Wilms et al. 2000), as demonstrated for several sources from detailed X-ray spectral analysis which revealed Compton-thick or near Compton-thick absorption (Lansbury et al. 2015). Several of the AGNs are even undetected in the X-ray band and are presumably heavily Compton thick, although deeper X-ray observations and further analyses would be required to confirm this. We caution that, although mid-infrared–X-ray analyses provide evidence for Compton-thick absorption, detailed X-ray spectral analyses are required to provide definitive proof (e.g., Georgantopoulos et al. 2011; Mateos et al. 2015; Del Moro et al. 2016).

As may be expected, our census of AGN activity is less complete in the distant Universe than found locally. How-

² The infrared emission is often not heavily obscured and so typically does not need to be corrected for obscuration.

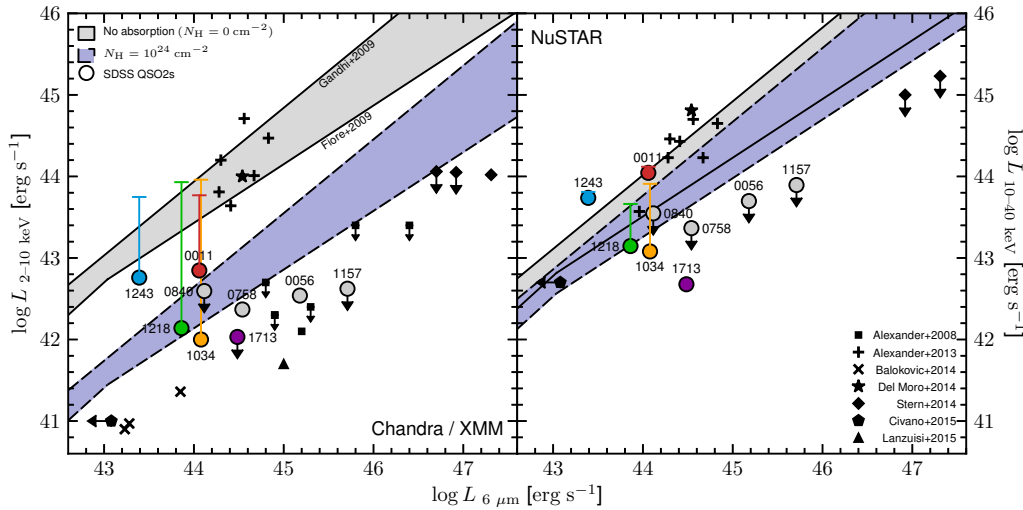


Fig. 2 Observed X-ray luminosity versus rest-frame $6 \mu\text{m}$ luminosity ($\nu L_{6\mu\text{m}}$) in both the rest-frame 2–10 keV (left; from *Chandra* and *XMM-Newton*) and rest-frame 10–40 keV (right; from *NuSTAR*) bands for a wide variety of AGNs (see Lansbury et al. 2015 for more details). The solid curves indicate the expected intrinsic (i.e., corrected for the presence of absorption) L_X – $L_{6\mu\text{m}}$ relationship from two different studies (Gandhi et al. 2009; Fiore et al. 2009) while the grey shaded region indicates the difference in expectations between these two studies. The dashed curves and solid purple region show the effect of Compton-thick absorption ($N_{\text{H}} = 10^{24} \text{ cm}^{-2}$) on the observed X-ray emission. Taken from Lansbury et al. (2015).

ever, surprisingly, we still lack a complete census of even luminous AGN activity within our own cosmic backyard ($d < 15 \text{ Mpc}$)! An example is the AGN in NGC 1448, which lies at a distance of just $\approx 12 \text{ Mpc}$ but was only discovered when observed with sensitive mid-infrared spectroscopy, which revealed the presence of a high-excitation [NeV] $14.3 \mu\text{m}$ emission line, the smoking gun evidence of AGN activity (Goulding & Alexander 2009). From the combination of *XMM-Newton*, *Chandra*, and *NuSTAR* X-ray spectral fitting with high-spatial resolution ground-based mid-infrared imaging it is now clear that the AGN in NGC 1448 is Compton thick, with a column density of $N_{\text{H}} > 5 \times 10^{24} \text{ cm}^{-2}$ (Annuar et al. submitted). Indeed, it seems likely that up to half of the AGN population in the local Universe is Compton thick (e.g., Burlon et al. 2011; Ricci et al. 2015). The fraction of the AGN population that are Compton thick in the distant Universe is significantly more uncertain; however, current results suggest that the fraction is broadly comparable with that seen locally, at least for AGNs of comparable luminosity (e.g., Aird et al. 2015; Buchner et al. 2015; Lanzuisi et al. 2015; Del Moro et al. 2016).

3 X-ray and infrared synergy: the connection between AGN activity and star formation

The combination of X-ray and infrared observations allow for the study of the connection between AGN activity and SF (e.g., from the measurement of AGN and SF activity in the X-ray and infrared bands, respectively). To first order we should expect a connection between AGN activity and SF

since both processes are driven by essentially the same gas supply: cold gas. SF is most efficient in cold dense molecular clouds, where gravity can overcome the kinetic energy of the gas and cause regions within the cloud to collapse and form stars. The gas that resides in the AGN accretion disc, with a temperature of $T \approx 10^5 \text{ K}$ is not typically considered cold! However, the majority of the gas would have originally been cold gas in the host galaxy and driven into the vicinity of the accretion disc (e.g., from the loss of angular momentum and/or stellar/supernovae winds and outflows; Jogee 2006) and then heated to high temperatures from viscosity in the accretion disc.

Tight relationships between the properties of the galaxy and the central supermassive black hole (e.g., Kormendy & Ho 2013; Graham 2016) potentially suggest a more symbiotic AGN–SF connection, whereby the growth of the black hole and the galaxy are somehow regulated (e.g., due to inflows or outflows from the galaxy; Alexander & Hickox 2012; Fabian 2012; King & Pounds 2015). Indeed, as shown in Fig. 3, the cosmological evolution in SF rate density and accretion rate density are remarkably similar, with an offset of a factor of ≈ 1500 , which is broadly the average ratio between the mass of the black hole and the galaxy spheroid for local galaxies. These results provide evidence for a global AGN–SF connection; however, they yield limited clues on the nature of the AGN–SF connection, such as whether there are dependencies on the AGN and SF luminosity.

Prior to the launch of *Herschel* in 2010, studies on the SF properties of distant X-ray AGNs were restricted to relatively low sensitivity instruments or observations that were

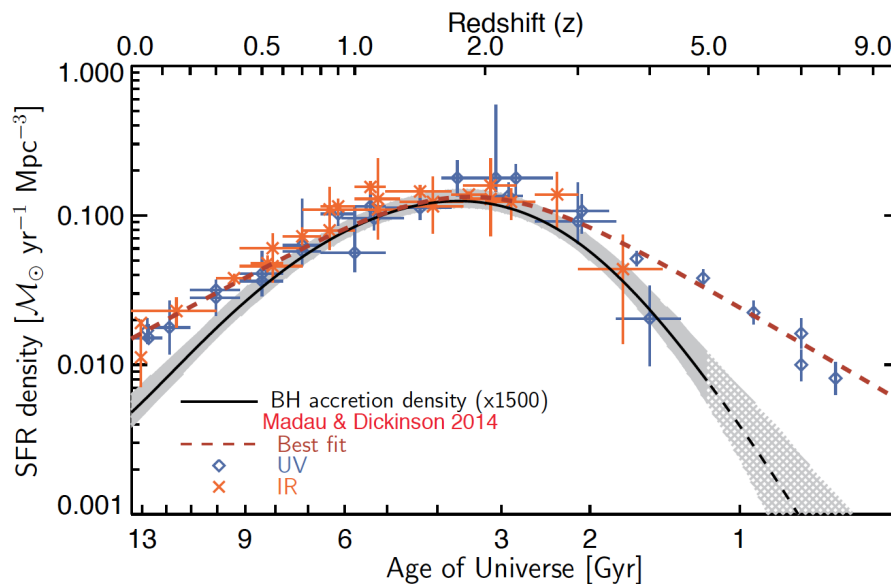


Fig. 3 SF rate density per unit volume versus cosmic time for galaxies, using either infrared or ultra-violet measurements (as indicated); the best-fitting relationship is indicated by a dashed curve. The accretion rate density from X-ray AGNs is also shown as a black curve (uncertainties indicated by the grey shaded region) but scaled up by a factor of 1500. Taken from Aird et al. (2015) using SF data from Madau & Dickinson (2014).

not optimal for reliable measurements of the SF properties (e.g., see §5.5 of Alexander & Hickox 2012). *Herschel*, and more recently ALMA, have greatly pushed forward our understanding of the AGN–SF connection by providing sensitive observations at far-infrared wavelengths, where the emission from dust-obscured SF peaks. From a suite of studies performed with *Herschel* (often including mid-infrared data from *Spitzer*) several key results on the SF properties of X-ray AGNs have crystallised (e.g., Harrison et al. 2012; Mullaney et al. 2012a,b; Chen et al. 2013; Rosario et al. 2013; DelVecchio et al. 2014; Stanley et al. 2015): (1) the mean SF luminosity and the mean specific SF rate (i.e., the stellar mass divided by the SF rate, a measure of how quickly the galaxy is growing) and their evolution with redshift are consistent with the SF galaxy population, (2) the mean SF luminosity of X-ray AGNs is flat with AGN luminosity, and (3) the mean AGN luminosity of infrared-selected SF galaxies correlates with the SF luminosity.

The first and third results imply a clear connection between AGN activity and SF, in agreement with the similar shapes of the accretion and SF rate densities; see Fig. 3. However, the second result appears to imply a lack of a connection. How can the observed relationship between AGN luminosity and SF luminosity depend on whether you calculate the mean SF luminosity from the AGN population or the mean AGN luminosity from the SF population? The likely answer lies in the timescales of stability between AGN activity and SF (e.g., Mullaney et al. 2012b; Gabor & Bournaud 2013; Hickox et al. 2014). AGNs are known to vary by factors of several on short timescales (measured in hours to years) and are likely to vary by orders of magnitude on longer timescales (measured in thousands to millions of

years) due to changes in the Eddington ratio (i.e., the mass accretion rate relative to the black-hole mass). By comparison, SF is more stable on short timescales and probably only varies significantly on timescales of $> 10^7$ years. Therefore, over the duration of a SF episode, the observed AGN luminosity at a given time could differ from the mean AGN luminosity by several orders of magnitude while the SF luminosity would be comparatively stable. A consequence of this would be a correlation between AGN and SF luminosity, if the AGN luminosity is averaged as a function of SF luminosity (the more stable quantity), and the absence of a correlation, if the SF luminosity is averaged as a function of AGN luminosity (the more variable quantity). These basic results are illustrated in the example study shown in Fig. 4. This figure shows the mean SF luminosity as a function of AGN luminosity and redshift for X-ray AGNs and also plots on the prediction for a simple model whereby the AGN and SF luminosities are correlated on long timescales but where the AGN luminosity can vary on short timescales. The AGN variability prescription is taken from the Eddington-ratio distribution of Aird et al. (2012), also plotted on Fig. 4. To first order, the good agreement between the simple model and the data suggests that the basic hypothesis is correct. However, we must be cautious about deriving more detailed conclusions from this comparison since (1) we have only assumed a simple model and other factors may play a role and (2) we have only been dealing with average quantities.

The results presented so far have been based on mean quantities because *Herschel* is not sensitive enough to individually detect a large fraction of the distant X-ray AGN population. For a typical log-normal distribution, the mean quantity will be biased towards the brightest sources and

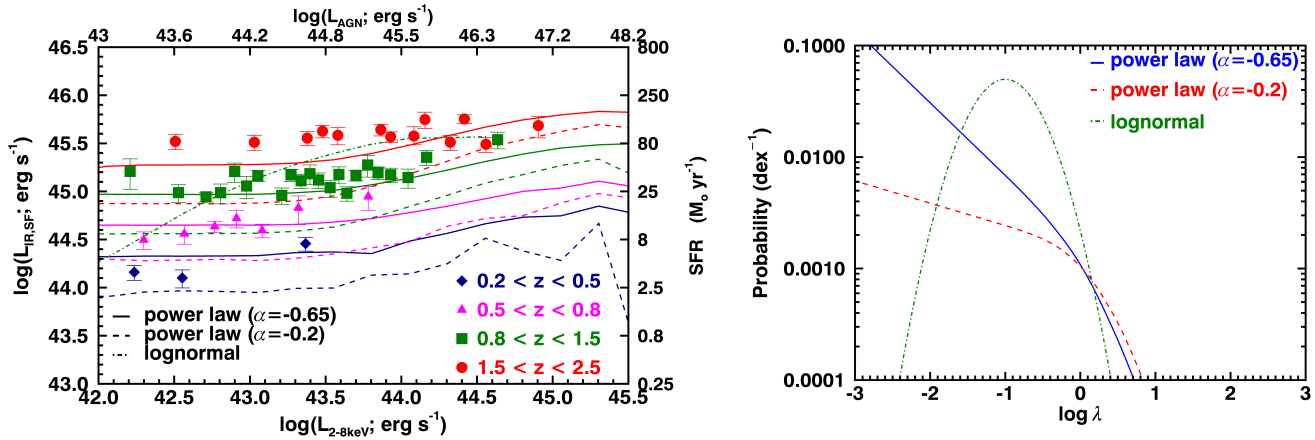


Fig. 4 (left) Mean infrared luminosity from SF ($L_{\text{IR,SF}}$) versus X-ray luminosity for X-ray selected AGNs over four redshift ranges. $L_{\text{IR,SF}}$ is calculated over 8–1000 μm and has been corrected for the infrared luminosity from the AGN by decomposing the infrared SED into AGN and SF components. The infrared luminosity to SF rate conversion is from Kennicutt (1998) and the bolometric AGN luminosity (L_{AGN}) is calculated from the X-ray luminosity using the luminosity dependent relation in Stern (2015). Predicted $L_{\text{IR,SF}}-L_{\text{AGN}}$ tracks for different model prescriptions of the Eddington-ratio distribution (as shown right) are plotted. Taken from Stanley et al. (2015).

will not be representative of a typical source. Thankfully, improved SF luminosity constraints can be obtained for individual X-ray AGNs using ALMA, which has significantly improved sensitivity over *Herschel* at rest-frame far-infrared wavelengths for AGNs and galaxies at $z > 1$. The first results for X-ray AGNs from ALMA are shown in Fig. 5. Despite the up-to an order of magnitude greater sensitivity of ALMA over *Herschel*, the majority of the X-ray AGNs are still undetected by ALMA (Mullaney et al. 2015). However, the ALMA upper limits are sensitive enough to demonstrate that the distribution of specific SF rates for the X-ray AGNs are inconsistent with that found for SF galaxies. The conclusion from this work is therefore that not all distant X-ray AGNs reside in SF galaxies, and that a substantial fraction (up-to $\approx 50\%$; Mullaney et al. 2015) are hosted in relatively quiescent galaxies with low levels of SF; qualitatively similar results are found for X-ray AGNs in the local Universe, using *Herschel* and the high-energy (15–194 keV) *Swift*-BAT survey (Shimizu et al. 2015). One exciting explanation for the significant fraction of X-ray AGNs in quiescent galaxies is that the SF has been shut off or suppressed by AGN-driven outflows. However, it would be premature to reach that conclusion from these data alone and other scenarios (e.g., due to the gas-inflow timescale, the accretion may proceed a long time after the start and end of the SF episode) could also explain the data.

4 Future prospects over the next decade

The most significant new observatory on the immediate horizon for X-ray–infrared synergy studies of AGNs is the *James Webb Space Telescope* (*JWST*) (Gardner et al. 2006), with an expected launch in 2018. With high sensitivity,

Hubble Space Telescope-like spatial imaging quality, and spectroscopy (integrated and spatially resolved) at infrared wavelengths of $\approx 0.6\text{--}28 \mu\text{m}$, *JWST* promises to break new ground in both of the science themes explored here. From the combination of *JWST* and *XMM-Newton*, *Chandra*, and *NuSTAR*, we should anticipate great advances in measuring the combined infrared and X-ray properties of AGNs and in completing the overall census of AGN activity. While the mid-infrared waveband does not probe the peak of the dust-obscured SF, *JWST* will also improve our constraints on the SF properties of X-ray AGNs by better identifying and constraining the AGN component either through high-spatial resolution imaging or spectroscopy. At the end of the next decade, *Athena* (Nandra et al. 2013) will launch (expected launch in 2028) and usher in a new era of X-ray astronomy. With unsurpassed X-ray spectral resolution and high sensitivity over a large field of view, *Athena* will dramatically push forward our census of the AGN population and our understanding of the connection of AGN activity with SF. However, *Athena* is unlikely to overlap with *JWST* (which has an expected lifetime of $\approx 5\text{--}10$ yrs) and, therefore, to optimise the impact and discovery potential, the current suite of X-ray observatories (*XMM-Newton*; *Chandra*; *NuSTAR*) will need to be operational over the lifetime of *JWST*.

Acknowledgements. I thank the substantial number of long-suffering collaborators who have worked with me over the last decade in Durham and beyond for their inspiring scientific discussions and research. I also thank the referee for a concise and constructive report. I acknowledge the Science and Technology Facilities Council (STFC) for support through grant ST/L00075X/1.

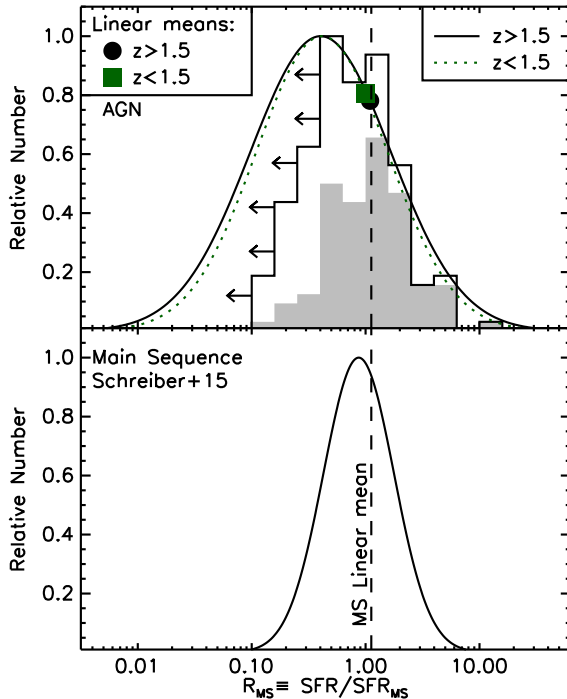


Fig. 5 SF rate distributions for distant X-ray AGNs with ALMA constraints (top) and the SF galaxy population (bottom; from Schreiber et al. 2015). The plotted distributions are the offset from the average of the SF galaxy population (i.e., the average of the main sequence: SFR_{MS} ; e.g., Schreiber et al. 2015) and take account of the host-galaxy mass. The solid grey histogram shows the SF properties of the ALMA-detected AGNs, the open histogram shows the SF properties of the AGNs with ALMA upper limits, while the solid and dotted curves show the best-fitting log-normal distributions for X-ray AGNs at $z > 1.5$ and $z < 1.5$, respectively, taking account of the detections and upper limits. The solid circle and solid square show the mean values, which are in agreement with the mean of the SF galaxy population; however, the peaks of the distributions are shifted to lower SF luminosities, indicating that not all X-ray AGNs reside in SF galaxies. Taken from Mullaney et al. (2015).

References

Aird, J., Coil, A. L., Moustakas, J., et al. 2012, *ApJ*, 746, 90
 Aird, J., Coil, A. L., Georgakakis, A., et al. 2015, *MNRAS*, 451, 1892
 Alexander, D. M., & Hickox, R. C. 2012, *NARev*, 56, 93
 Alexander, D. M., Chary, R.-R., Pope, A., et al. 2008, *ApJ*, 687, 835-847
 Asmus, D., Gandhi, P., Hönig, S. F., Smette, A., & Duschl, W. J. 2015, *MNRAS*, 454, 766
 Assef, R. J., Stern, D., Kochanek, C. S., et al. 2013, *ApJ*, 772, 26
 Bauer, F. E., Yan, L., Sajina, A., & Alexander, D. M. 2010, *ApJ*, 710, 212
 Brandt, W. N., & Alexander, D. M. 2015, *A&ARv*, 23, 1
 Buchner, J., Georgakakis, A., Nandra, K., et al. 2015, *ApJ*, 802, 89
 Burlon, D., Ajello, M., Greiner, J., et al. 2011, *ApJ*, 728, 58

Chen, C.-T. J., Hickox, R. C., Alberts, S., et al. 2013, *ApJ*, 773, 3
 Del Moro, A., Alexander, D. M., Bauer, F. E., et al. 2016, *MNRAS*, 456, 2105
 Delvecchio, I., Lutz, D., Berta, S., et al. 2015, *MNRAS*, 449, 373
 Done, C. 2010, arXiv:1008.2287
 Donley, J. L., Koekemoer, A. M., Brusa, M., et al. 2012, *ApJ*, 748, 142
 Elitzur, M., & Shlosman, I. 2006, *ApJ*, 648, L101
 Fabian, A. C. 2012, *ARA&A*, 50, 455
 Fiore, F., Puccetti, S., Brusa, M., et al. 2009, *ApJ*, 693, 447
 Gabor, J. M., & Bournaud, F. 2013, *MNRAS*, 434, 606
 Gandhi, P., Horst, H., Smette, A., et al. 2009, *A&A*, 502, 457
 Gardner, J. P., Mather, J. C., Clampin, M., et al. 2006, *SSRv*, 123, 485
 Georgantopoulos, I., Rovilos, E., Akylas, A., et al. 2011, *A&A*, 534, A23
 Georgantopoulos, I., Comastri, A., Vignali, C., et al. 2013, *A&A*, 555, A43
 Goulding, A. D., & Alexander, D. M. 2009, *MNRAS*, 398, 1165
 Graham, A. W. 2016, *Galactic Bulges*, 418, 263
 Hardcastle, M. J., Evans, D. A., & Croston, J. H. 2009, *MNRAS*, 396, 1929
 Harrison, C. M., Alexander, D. M., Mullaney, J. R., et al. 2012, *ApJ*, 760, L15
 Harrison, F. A., Craig, W. W., Christensen, F. E., et al. 2013, *ApJ*, 770, 103
 Hickox, R. C., Mullaney, J. R., Alexander, D. M., et al. 2014, *ApJ*, 782, 9
 Jansen, F., Lumb, D., Altieri, B., et al. 2001, *A&A*, 365, L1
 Jøgee, S. 2006, *Physics of Active Galactic Nuclei at all Scales*, 693, 143
 Kennicutt, R. C., Jr. 1998, *ARA&A*, 36, 189
 Kennicutt, R. C., & Evans, N. J. 2012, *ARA&A*, 50, 531
 King, A., & Pounds, K. 2015, *ARA&A*, 53, 115
 Kormendy, J., & Ho, L. C. 2013, *ARA&A*, 51, 511
 Lansbury, G. B., Gandhi, P., Alexander, D. M., et al. 2015, *ApJ*, 809, 115
 Lanzuisi, G., Ranalli, P., Georgantopoulos, I., et al. 2015, *A&A*, 573, A137
 López-Gonzaga, N., Burtscher, L., Tristram, K. R. W., Meisenheimer, K., & Schartmann, M. 2016, *A&A*, 591, A47
 Lutz, D. 2014, *ARA&A*, 52, 373
 Madau, P., & Dickinson, M. 2014, *ARA&A*, 52, 415
 Mateos, S., Alonso-Herrero, A., Carrera, F. J., et al. 2012, *MNRAS*, 426, 3271
 Mateos, S., Carrera, F. J., Alonso-Herrero, A., et al. 2015, *MNRAS*, 449, 1422
 Mullaney, J. R., Pannella, M., Daddi, E., et al. 2012a, *MNRAS*, 419, 95
 Mullaney, J. R., Daddi, E., Béthermin, M., et al. 2012b, *ApJ*, 753, L30
 Mullaney, J. R., Alexander, D. M., Aird, J., et al. 2015, *MNRAS*, 453, L83
 Nandra, K., Barret, D., Barcons, X., et al. 2013, arXiv:1306.2307
 Pilbratt, G. L., Riedinger, J. R., Passvogel, T., et al. 2010, *A&A*, 518, L1
 Ricci, C., Ueda, Y., Koss, M. J., et al. 2015, *ApJ*, 815, L13
 Rosario, D. J., Santini, P., Lutz, D., et al. 2013, *ApJ*, 771, 63
 Sazonov, S., Willner, S. P., Goulding, A. D., et al. 2012, *ApJ*, 757, 181
 Schreiber, C., Pannella, M., Elbaz, D., et al. 2015, *A&A*, 575, A74
 Shimizu, T. T., Mushotzky, R. F., Meléndez, M., Koss, M., & Rosario, D. J. 2015, *MNRAS*, 452, 1841

- Stanley, F., Harrison, C. M., Alexander, D. M., et al. 2015, MN-RAS , 453, 591
- Stern, D., Assef, R. J., Benford, D. J., et al. 2012, ApJ , 753, 30
- Stern, D. 2015, ApJ , 807, 129
- Tristram, K. R. W., Burtscher, L., Jaffe, W., et al. 2014, A&A, 563, A82
- Weisskopf, M. C., Brinkman, B., Canizares, C., et al. 2002, PASP , 114, 1
- Wilms, J., Allen, A., & McCray, R. 2000, ApJ , 542, 914